Robust Iterative Method for Nonlinear Helmholtz Equation☆

Lijun Yuan[a,*], Ya Yan Lu[b]

[a] *College of Mathematics and Statistics, Chongqing Technology and Business University, Chongqing 400067, China*
[b] *Department of Mathematics, City University of Hong Kong, Kowloon, Hong Kong*

Abstract

A new iterative method is developed for solving the two-dimensional nonlinear Helmholtz equation which governs polarized light in media with the optical Kerr nonlinearity. In the strongly nonlinear regime, the nonlinear Helmholtz equation could have multiple solutions related to phenomena such as optical bistability and symmetry breaking. The new method exhibits a much more robust convergence behavior than existing iterative methods, such as frozen-nonlinearity iteration, Newton's method and damped Newton's method, and it can be used to find solutions when good initial guesses are unavailable. Numerical results are presented for the scattering of light by a nonlinear circular cylinder based on the exact nonlocal boundary condition and a pseudospectral method in the polar coordinate system.

Keywords: Helmholtz equation, Wave propagation, Kerr nonlinearity, Iterative method, Optical bistability.

1. Introduction

Wave propagation in a medium where the effective permittivity varies with the intensity of the wave, can often be modeled by a scalar nonlinear

☆This work was supported by the National Natural Science Foundation of China (11201508), the Natural Science Foundation of Chongqing (cstc2016jcyjA0491), and the Research Grants Council of Hong Kong (CityU 11301914).

*Corresponding author.

Email addresses: ljyuan@ctbu.edu.cn (Lijun Yuan), mayylu@cityu.edu.hk (Ya Yan Lu)

Helmholtz equation (NLH) [1]. For electromagnetic waves and light, the NLH can be derived from the nonlinear Maxwell's equations with a third order nonlinearity, under the assumptions that the electric field is linearly polarized and third harmonic generation can be ignored [1, 2, 3]. The equation has been used to analyze important nonlinear optical effects, such as optical bistability [4, 5, 6, 7, 8], spatial solitons [9], self-focusing of laser beams [10, 11, 12, 13], symmetry breaking [14, 15, 16, 17, 18], etc. Since the nonlinear coefficient of a typical medium is very small, the nonlinear effects are only significant if the field intensity is very high or the interaction length (for example, along an optical fiber) is very long. In recent years, many optical microcavities with very high quality factors and small mode volumes have been fabricated and used to enhance nonlinear optical effects [19]. Potentially significant applications, such as ultra-small optical switches with very low operating powers may be realized based on enhanced nonlinear effects in microcavities [20]. To analyze these structures, it is important to have efficient numerical methods for solving the NLHs and the more general nonlinear Maxwell's equations in the strongly nonlinear regime.

Boundary value problems of the NLH could have multiple solutions related to optical bistability, symmetry breaking, etc. Due to the nonlinearity, all numerical methods are iterative. The one-dimensional NLH can be easily solved by a shooting method where the iterations are performed on a single parameter at the boundary [21, 22, 23, 24]. The two-dimensional (2D) and three-dimensional (3D) NLHs are much more difficult to solve, since the iterations are performed on the solutions defined on the entire domain. Existing iterative schemes include the frozen-nonlinearity iteration, Newton's method, the damped Newton's method, etc [25]. The frozen-nonlinearity iteration converges to a solution very slowly, and often fails to converge, especially when there are multiple solutions. Newton's method has a fast quadratic convergence rate, but its domain of convergence is often too small.

In this paper, we develop a new iterative method for the 2D NLH in the strongly nonlinear regime. Like the damped Newton's method, our method has a linear convergence rate, but it appears to have a very large convergence domain and it does not involve any parameters. The method is easier to implement than Newton's method. It can be used to find the solutions of the NLH directly, or find good approximations that can be further improved by Newton's method. To illustrate the method, we analyze the scattering of plane incident waves by a nonlinear circular cylinder, and consider the strongly nonlinear regime where the problem has multiple solutions.

2. Formulation and linear properties

We consider the following 2D NLH:

$$\frac{\partial^2 u}{\partial x^2} + \frac{\partial^2 u}{\partial y^2} + k_0^2(\varepsilon + \gamma|u|^2)u = 0, \tag{1}$$

where $k_0 = \omega/c$ is the free space wavenumber, ω is the angular frequency, c is the speed of light in vacuum, $\varepsilon = \varepsilon(x, y)$ is the relative permittivity (dielectric function), $\gamma = \gamma(x, y)$ is the nonlinear coefficient, u is the z component of the electric field, and the time dependence is $\exp(-\mathrm{i}\omega t)$. We further assume that the nonlinear structure is a circular cylinder of radius a surrounded by a linear homogeneous medium with

$$\varepsilon(x, y) = \varepsilon_0 > 0, \ \gamma(x, y) = 0, \quad r > a, \tag{2}$$

where $r = \sqrt{x^2 + y^2}$.

In the homogeneous medium outside the nonlinear cylinder, we specify a plane incident wave

$$u^{(i)}(x, y) = Ae^{\mathrm{i}k_0 n_0 x}, \quad r > a, \tag{3}$$

where $n_0 = \sqrt{\varepsilon_0}$ is the refractive index of the medium and A is the amplitude of the incident wave. The total field outside the cylinder is the sum of $u^{(i)}$ and the scattered wave $u^{(s)}$, and $u^{(s)}$ can be expanded in outgoing cylindrical waves as

$$u^{(s)}(x, y) = \sum_{m=-\infty}^{\infty} c_m H_m^{(1)}(k_0 n_0 r) e^{\mathrm{i}m\theta}, \quad r > a, \tag{4}$$

where θ is the polar angle, $H_m^{(1)}$ is the Hankel function of the first kind and order m.

It is possible to introduce a nonlocal boundary condition at $r = a$, so that Eq. (1) can be solved on the disk of radius a. Let Λ be a linear operator acting on 2π-periodic functions of θ such that

$$\Lambda e^{\mathrm{i}m\theta} = \lambda_m e^{\mathrm{i}m\theta}, \quad \lambda_m = k_0 n_0 \frac{H_m^{(1)\prime}(k_0 n_0 a)}{H_m^{(1)}(k_0 n_0 a)} \tag{5}$$

for all integers m, where $H_m^{(1)\prime}$ is the derivative of $H_m^{(1)}$, then it is easy to verify that $\partial_r u^{(s)} = \Lambda u^{(s)}$ at $r = a^+$. At $r = a$, u is continuous since it is a

tangential component (the z component) of the electric field along the surface of the cylinder. Meanwhile, $\partial u/\partial r$ is also continuous, since it is related to the horizontal components of the magnetic field which are always continuous. Therefore, we obtain the following well-known Dirichlet-to-Neumann (DtN) boundary condition

$$\frac{\partial u}{\partial r} = \Lambda u + Ah, \quad r = a, \tag{6}$$

where $h = (\partial_r - \Lambda)e^{\mathrm{i}k_0 n_0 x}|_{r=a}$ is a function of θ. Using this condition, it is only necessary to solve Eq. (1) on the disk $\Omega = \{(x, y) : r < a\}$.

If the cylinder is linear and homogeneous, i.e., $\varepsilon(x, y) = \varepsilon_1 > 0$ and $\gamma(x, y) = 0$ for $r < a$, then the scattering problem can be solved analytically. The field inside the cylinder can be expanded as

$$u(x, y) = \sum_{m=-\infty}^{\infty} b_m J_m(k_0 n_1 r) e^{\mathrm{i}m\theta}, \quad r < a, \tag{7}$$

where $n_1 = \sqrt{\varepsilon_1}$, and J_m is the Bessel function of the first kind and order m. The coefficients b_m and c_m can be solved analytically. Based on the solution, we can calculate the scattered power P_s by integrating the real part of the r component of the complex Poynting vector (of the scattered field) along the circle $r = a$. To obtain the normalized scattered power, we divide P_s by the intensity of the incident field $I_{in} = A^2 n_0/Z_0$ where Z_0 is the free space impedance, and by the diameter of the cylinder $2a$. In Fig. 1, we show the normalized scattered power as a function of the normalized frequency $\omega L/(2\pi c) = k_0 L/(2\pi)$, where $L = 1\,\mu$m, for a dielectric cylinder surrounded by air. The radius and the dielectric constant of the cylinder are $a = 0.4L$ and $\varepsilon_1 = 6.25$, respectively, and the dielectric constant of air is $\varepsilon_0 = 1$.

The peaks in Fig. 1 correspond to the resonant frequencies. The resonant modes are nontrivial solutions of the linear homogeneous Helmholtz equation satisfying the exact outgoing DtN boundary condition, i.e., Eq. (6) with $A = 0$. They exist at a discrete sequence of complex frequencies. The real part of a complex frequency is the resonant frequency, and the imaginary part is the decay rate in time. The resonant modes are solutions of an improper eigenvalue problem. Since k_0 is complex, these modes actually blow up at infinity. In Fig. 1, the third peak corresponds to a resonant mode with the complex frequency $\omega_* L/(2\pi c) = 0.9779 - 0.0087\mathrm{i}$. In Fig. 2, we show the magnitude of the total field for an incident plane wave with $\omega L/(2\pi c) = 0.9779$. Notice that the field is enhanced by a factor about 4.

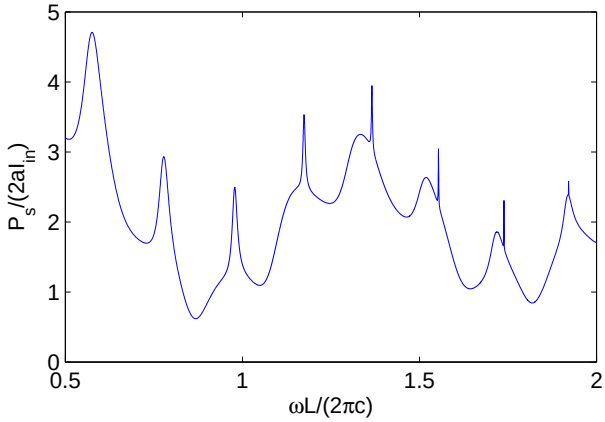

Figure 1: Normalized scattered power, $P_s/(2aI_{in})$, as a function of the normalized frequency for a linear dielectric cylinder illuminated by a plane incident wave.

3. Iterative methods

To solve Eq. (1), an iterative method is needed. The simplest iterative method may be the frozen-nonlinearity iteration

$$\mathcal{L}u^{(l+1)} + k_0^2\gamma|u^{(l)}|^2u^{(l+1)} = 0, \tag{8}$$

where $\mathcal{L} = \partial_x^2 + \partial_y^2 + k_0^2\varepsilon$, $u^{(l)}$ is the current iteration (or initial guess if $l = 0$), $u^{(l+1)}$ is the next iteration to be determined. Notice that Eq. (8) is a linear Helmholtz equation for $u^{(l+1)}$, and it should be solved with the boundary condition (6).

The frozen-nonlinearity iteration converges very slowly and often fails to converge, especially when the nonlinear effect is strong. A much better alternative is Newton's method. Since both u and its complex conjugate $\overline{u}$ appear in the NLH, we re-write Eq. (1) as

$$f(u, \overline{u}) = \mathcal{L}u + k_0^2\gamma u^2\overline{u} = 0. \tag{9}$$

Assuming $u = u^{(l)} + s$, where s is small, Eq. (9) is approximated by

$$f(u^{(l)}, \overline{u}^{(l)}) + \frac{\partial f}{\partial u}(u^{(l)}, \overline{u}^{(l)})s + \frac{\partial f}{\partial \overline{u}}(u^{(l)}, \overline{u}^{(l)})\overline{s} = 0, \tag{10}$$

where

$$\frac{\partial f}{\partial u}(u, \overline{u}) = \mathcal{L} + 2k_0^2\gamma|u|^2, \quad \frac{\partial f}{\partial \overline{u}}(u, \overline{u}) = k_0^2\gamma u^2.$$

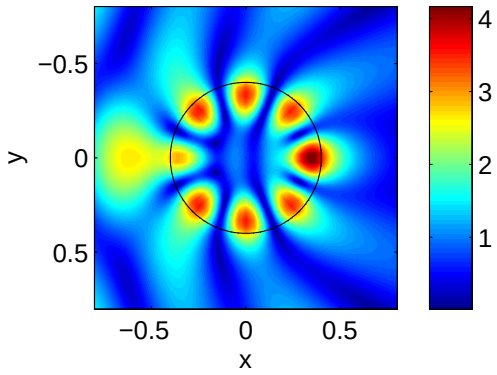

Figure 2: Magnitude of the wave field excited by a plane wave with amplitude $A = 1$ and frequency $\omega L/(2\pi c) = 0.9779$.

Newton's method is simply

$$u^{(l+1)} = u^{(l)} + s, \tag{11}$$

where s must be solved from Eq. (10). An explicit version of Newton's method for Eq. (1) is

$$\mathcal{L}u^{(l+1)} + k_0^2\gamma\left\{2|u^{(l)}|^2u^{(l+1)} + [u^{(l)}]^2\overline{u}^{(l+1)}\right\} = 2k_0^2\gamma|u^{(l)}|^2u^{(l)}. \tag{12}$$

Since $\overline{u}^{(l+1)}$ appears in Eq. (12), it is necessary to solve an equivalent system of two partial differential equations for the real and imaginary parts of $u^{(l+1)}$. Newton's method converges rapidly due to its quadratic convergence. However, it only converges if the initial guess is sufficiently close to the exact solution. To enlarge the domain of convergence, it is often useful to use the damped Newton's method

$$u^{(l+1)} = u^{(l)} + \eta s, \tag{13}$$

where η is a damping parameter between 0 and 1. The explicit version of the damped Newton's method is

$$\begin{aligned}\mathcal{L}u^{(l+1)} + k_0^2\gamma\left\{2|u^{(l)}|^2u^{(l+1)} + [u^{(l)}]^2\overline{u}^{(l+1)}\right\}\\ = (1-\eta)\mathcal{L}u^{(l)} + (3-\eta)k_0^2\gamma|u^{(l)}|^2u^{(l)}.\end{aligned} \tag{14}$$

The simplest damped Newton's method is to choose η as a constant in all iterations. In that case, the method has a linear convergence rate. However,

it is often difficult to choose a proper η for practical applications. Therefore, the damped Newton's method is often implemented so that $||f||$ decreases in each iteration [25]. The so-called Armijo rule determines η as the largest number in a decreasing sequence (e.g., $\{1, 1/3, 1/9, 1/27, ...\}$), such that

$$||f(u^{(l+1)}, \overline{u}^{(l+1)})|| < (1 - \alpha\eta)||f(u^{(l)}, \overline{u}^{(l)})||, \tag{15}$$

where α is a small positive constant (e.g., $\alpha = 10^{-4}$) and $u^{(l+1)}$ is the next iteration given in Eq. (13) for the accepted η.

Replacing $\overline{u}^{(l+1)}$ in Eq. (12) by $\overline{u}^{(l)}$, we obtain the following iterative method

$$\mathcal{L}u^{(l+1)} + 2k_0^2\gamma|u^{(l)}|^2u^{(l+1)} = k_0^2\gamma|u^{(l)}|^2u^{(l)}. \tag{16}$$

To the best of our knowledge, the above is not a special case of any existing variations of Newton's method. Although it is very simple, the method is specially derived for the NLH with an approximation related to $\overline{u}$. In the following sections, we show that the above method is much more robust than Newton's method and damped Newton's method. Furthermore, since $\overline{u}^{(l+1)}$ has been avoided, Eq. (16) is easier to implement than Newton's method. Like the damped Newton's method with a constant damping parameter, the above method has a linear convergence rate. To obtain highly accurate solutions to the NLH, we can use the method to find a sufficiently accurate approximation, then further improve the solution by Newton's method.

4. Discretization

In this section, we briefly describe a numerical method for discretizing Eq. (1) and the iterative schemes Eqs. (8), (12), (14) and (16). Due to the circular geometry and the polar coordinate system, we use a mixed pseudospectral method with Chebyshev and Fourier collocations in the radial and angle directions, respectively [26]. To avoid the singularity at $r = 0$, the radial variable is extended to $[-a, a]$ by $u(r, \theta) = u(-r, \tilde{\theta})$ for $r < 0$, where $\tilde{\theta} = (\theta + \pi)\text{mod}(2\pi)$, so that the equations for u are supposed to be valid for $r \in (-a, a)$ and $\theta \in [0, 2\pi]$. However, the unknowns associated with the negative r will be eliminated, so that the final system is only related to u for $r > 0$.

Let $Q = 2N+1$ and M be two positive odd and even integers, respectively, we discretize the polar coordinates by

$$r_j = a\cos(j\pi/Q), \quad 0 \le j \le Q, \tag{17}$$

$$\theta_k = (2k-1)\pi/M, \quad 1 \le k \le M. \tag{18}$$

Let u_{jk} be the numerical approximation of $u(r_j, \theta_k)$, we introduce a column vector $\boldsymbol{u}_j = [u_{j1}, u_{j2}, ..., u_{jM}]^\mathsf{T}$ for unknowns on the circle of radius r_j, and the larger column vector

$$\boldsymbol{u} = [\boldsymbol{u}_1^\mathsf{T}, \boldsymbol{u}_2^\mathsf{T}, ..., \boldsymbol{u}_N^\mathsf{T}]^\mathsf{T} \tag{19}$$

for all unknowns inside the disk Ω.

For the partial derivative with respect to r, the Chebyshev collocation method gives rise to an $(Q+1) \times (Q+1)$ differentiation matrix that links a column vector of u_{jk} (for fixed k and $0 \leq j \leq Q$) to a corresponding vector approximating $\partial_r u(r_j, \theta_k)$. The second order derivative operator ∂_r^2 can be approximated by the square of that matrix. Similarly, the Fourier collocation method gives rise to an $M \times M$ differentiation matrix that links $\boldsymbol{u}_j$ to a vector approximating $\partial_\theta u(r_j, \theta_k)$ for fixed j and all k. Using these differentiation matrices, we can approximate Eq. (1) at (r_j, θ_k) for $1 \leq j < Q$ and $1 \leq k \leq M$. After eliminating the unknowns corresponding to $r < 0$, we obtain

$$(\mathcal{B} + \mathcal{D})\boldsymbol{u} + \mathcal{B}_0 \boldsymbol{u}_0 = \boldsymbol{0}, \tag{20}$$

where $\boldsymbol{u}_0$ is a vector for u on the circle $r = a$, $\mathcal{B}$ is an $(MN) \times (MN)$ matrix, $\mathcal{D} = \mathcal{D}(\boldsymbol{u})$ is a diagonal matrix with the diagonal entries $k_0^2 \gamma(r_j, \theta_k)|u_{jk}|^2$, and $\mathcal{B}_0$ is an $(MN) \times M$ matrix. Using the differentiation matrix for ∂_r at $j = 0$ and eliminating those unknowns for $r < 0$, the boundary condition (6) is discretized as

$$\mathcal{C}\boldsymbol{u} + \mathcal{C}_0 \boldsymbol{u}_0 = A\boldsymbol{h}, \tag{21}$$

where $\mathcal{C}$ is an $M \times (MN)$ matrix, $\mathcal{C}_0$ is an $M \times M$ matrix, and $\boldsymbol{h}$ is a column vector of $h(\theta_k)$ for $1 \leq k \leq M$. We can eliminate $\boldsymbol{u}_0$ from Eqs. (20) and (21), and obtain a nonlinear system for $\boldsymbol{u}$:

$$(\mathcal{F} + \mathcal{D})\boldsymbol{u} = A\boldsymbol{g}, \tag{22}$$

where $\mathcal{F}$ is an $(MN) \times (MN)$ matrix and $\boldsymbol{g}$ is a column vector related to the incident field. We can re-write Eq. (22) as $\boldsymbol{f}(\boldsymbol{u}) = \boldsymbol{0}$ where

$$\boldsymbol{f}(\boldsymbol{u}) = (\mathcal{F} + \mathcal{D})\boldsymbol{u} - A\boldsymbol{g} \tag{23}$$

and the dependence on $\overline{\boldsymbol{u}}$ is suppressed.

The above discretization scheme can be easily applied to the iterative methods given in Eqs. (8), (12), (14) and (16). For example, Newton's method (12) can be discretized as

$$[\mathcal{F} + 2\mathcal{D}^{(l)}]\boldsymbol{u}^{(l+1)} + \tilde{\mathcal{D}}^{(l)}\overline{\boldsymbol{u}}^{(l+1)} = 2\mathcal{D}^{(l)}\boldsymbol{u}^{(l)} + A\boldsymbol{g}, \tag{24}$$

where $\mathcal{D}^{(l)}$ is the diagonal matrix with diagonal entries $k_0^2\gamma(r_j,\theta_k)|u_{jk}^{(l)}|^2$, and $\tilde{\mathcal{D}}^{(l)}$ is a diagonal matrix with diagonal entries $k_0^2\gamma(r_j,\theta_k)[u_{jk}^{(l)}]^2$. The damped Newton's method can be discretized as

$$[\mathcal{F}+2\mathcal{D}^{(l)}]\boldsymbol{u}^{(l+1)}+\tilde{\mathcal{D}}^{(l)}\overline{\boldsymbol{u}}^{(l+1)}=[(1-\eta)\mathcal{F}+(3-\eta)\mathcal{D}^{(l)}]\boldsymbol{u}^{(l)}+\eta A\boldsymbol{g}. \quad (25)$$

The Armijo rule can be implemented with

$$||\boldsymbol{f}(\boldsymbol{u}^{(l+1)})||<(1-\alpha\eta)||\boldsymbol{f}(\boldsymbol{u}^{(l)})||, \quad (26)$$

where $||\cdot||$ is simply the vector 2-norm. Since $\overline{\boldsymbol{u}}^{(l+1)}$ appears in Eqs. (24) and (25), it is necessary to rewrite these two equations as real linear systems for $2MN$ unknowns, i.e., the real and imaginary parts of $\boldsymbol{u}^{(l+1)}$. The new iterative method given in Eq. (16) can be discretized as

$$[\mathcal{F}+2\mathcal{D}^{(l)}]\boldsymbol{u}^{(l+1)}=\mathcal{D}^{(l)}\boldsymbol{u}^{(l)}+A\boldsymbol{g}. \quad (27)$$

Notice that the above is a linear system for $\boldsymbol{u}^{(l+1)}$.

If we take advantage of the reflection symmetry with respect to the x axis, the number of unknowns in Eqs. (24), (25) and (27) can be further reduced by a factor of two. This leads to linear systems with only $MN/2$ unknowns, which are u_{jk} for $1\le j\le N$ and $1\le k\le M/2$.

5. Numerical results

In this section, we present numerical results for the scattering of a plane incident wave by a nonlinear circular cylinder. As in section 2, we assume $\varepsilon_1=6.25$, $\varepsilon_0=1$, and $a=0.4L$, where ε_1 and ε_0 are the dielectric constants of the cylinder and the surrounding medium, respectively, a is the radius of the cylinder, and $L=1\,\mu$m. The cylinder is assumed to have a constant nonlinear coefficient $\gamma_1=2\times10^{-12}\,\mathrm{m}^2/\mathrm{V}^2$. Since the plane incident wave given in Eq. (3) propagates in the x direction and the center of the cylinder is located at the origin, the problem has a reflection symmetry with respect to the x axis. However, this is a nonlinear boundary value problem, uniqueness cannot be guaranteed, and the solutions may or may not preserve the symmetry. In fact, for some parameter ranges, the problem has asymmetric solutions related to the symmetry breaking phenomenon [18]. Since our objective is to investigate the iterative methods for Eq. (1), we consider only the symmetric solutions which are even functions of y. Furthermore, although

we state the problem in physical units, our results can be easily scaled, and they depend on two dimensionless quantities $k_0 a$ and $\gamma_1|A|^2$, where A is the amplitude of the incident wave and k_0 is the free space wavenumber.

From the NLH, it is clear that strong nonlinear effects may be realized if $\gamma_1|u|^2$ (in the cylinder) is comparable with ε_1, i.e, $O(1)$. Since γ_1 is very small, the field must have a large amplitude in the nonlinear cylinder. The nonlinear effects can be enhanced by resonances, since the amplitude of the wave field in the resonator can be much larger than that of the incident wave. For a circular cylinder, the resonant frequencies (real part of the complex frequencies of the resonant modes) can be calculated analytically, and as functions of ε_1, they decrease as ε_1 is increased. Since γ_1 is positive, the nonlinear term $\gamma_1|u|^2$ has the effect of increasing the dielectric function ε. Therefore, the nonlinear effect is more significant when the frequency is slightly below a resonant frequency.

For the cylinder considered above, we recall that $\omega L/(2\pi c) = 0.9779$ is a resonant frequency. For the nonlinear case, we choose the normalized frequency $\omega L/(2\pi c) = 0.9346$ for which a strong optical bistability phenomenon occurs. In Fig. 3, we show the scattered power P_s versus the in-

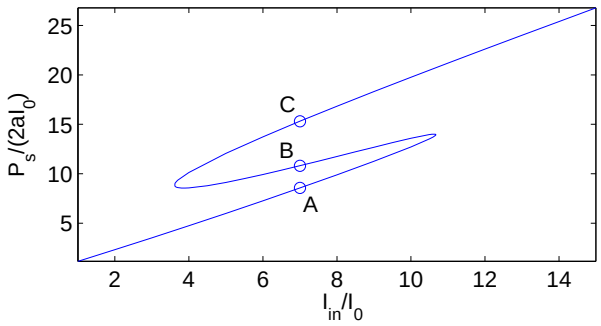

Figure 3: Normalized scattered power as the function of the normalized incident wave intensity at frequency $\omega L/(2\pi c) = 0.9346$.

tensity I_{in} of the incident wave. A reference incident wave with amplitude $A_0 = 10^5\,\mathrm{V/m}$ and intensity I_0 is introduced for scaling. The vertical and horizontal axes in Fig. 3 are $P_s/(2aI_0)$ and $I_{in}/I_0 = (A/A_0)^2$, respectively. For $3.62 \le I_{in}/I_0 \le 10.67$, the NLH has three solutions with different values of P_s. This corresponds to the optical bistability phenomenon, since the two solutions corresponding to the upper and lower branches in Fig. 3 are

presumably stable, and other solution is unstable. A rigorous stability analysis can be performed starting from the original time-dependent nonlinear Maxwell's equations. For $I_{in} = 7I_0$, i.e., $A = \sqrt{7}A_0$, the NLH has three solutions marked as A, B and C in Fig. 3. The electric field patterns of these solutions are shown in Fig. 4. These results are obtained using the new iter-

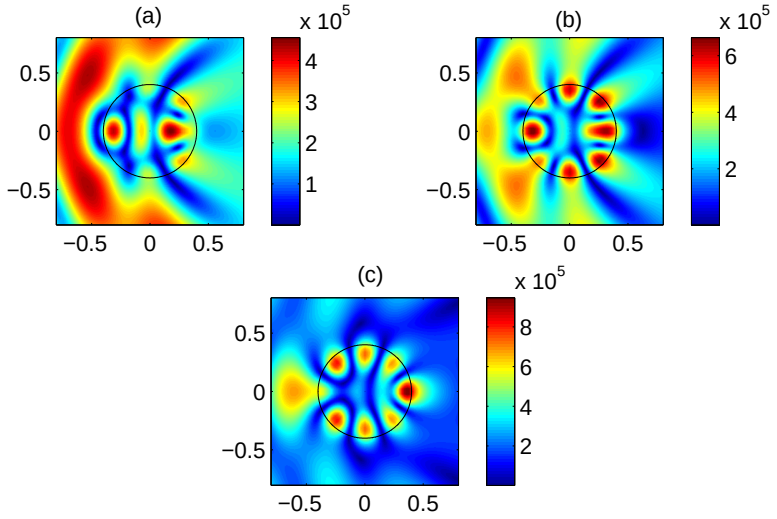

Figure 4: Wave field patterns (magnitude of u) of the three solutions marked as A, B and C in Fig. 3.

ative method given in Eq. (16) with $Q = 51$ and $M = 50$. In each iteration, we only need to solve a linear system with $(MN)/2 = 625$ unknowns.

6. Convergence behavior

In this section, we compare the iterative methods presented in section 3. The convergence behaviors of these methods are studied for two cases where the initial guess $\boldsymbol{u}^{(0)}$ is either zero or the converged solution for a slightly different incident wave. The stop criterion used in the iterations is

$$\max\left\{\frac{||\boldsymbol{u}^{(l)} - \boldsymbol{u}^{(l-1)}||}{||\boldsymbol{u}^{(l)}||}, \frac{||\boldsymbol{f}(\boldsymbol{u}^{(l)})||}{||A\boldsymbol{g}||}\right\} < 10^{-9}. \tag{28}$$

Notice that both terms in the curly brackets above are required to be small. The second term is the normalized residual for Eq. (22). The first term is

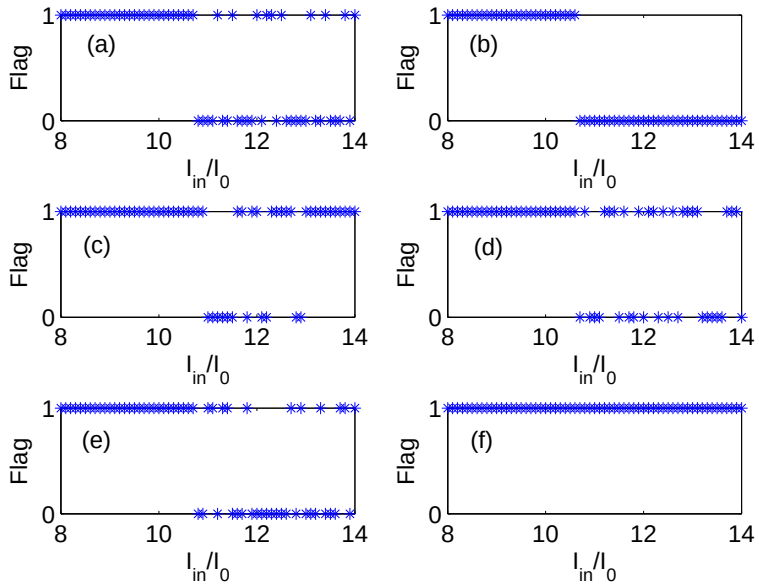

Figure 5: Convergence behaviors of the iterative methods for zero initial guess and incident wave intensity $I_{in} = (8 + 0.1k)I_0$, $k = 0, 1, 2, ..., 60$. A method is convergent if $\mathsf{Flag} = 1$, and non-convergent if $\mathsf{Flag} = 0$. (a) Newton's method; (b) damped Newton's method with Armijo rule; (c)-(e) damped Newton's method with constant parameter $\eta = 0.1$, 0.4 and 0.7, respectively; (f): our iterative method Eq. (16).

introduced to ensure that the iterations smoothly converge to a solution, instead of jumping on the solution accidentally. The maximum number of iterations is set to be 2000. If the stop criterion is not satisfied for all 2000 iterations, the iterative method is considered as non-convergent for the particular initial guess.

For a large range of the incident wave amplitude, we attempt to solve the NLH by various iterative methods starting from $\boldsymbol{u}^{(0)} = \mathbf{0}$. The convergence behaviors of Newton's method, damped Newton's method with Armijo rule (with parameter $\alpha = 10^{-4}$), damped Newton's method with constant parameter $\eta = 0.1$, 0.4 and 0.7, and our method given in Eq. (16) are shown in Figs. 5(a)-(f), respectively. As in the last section, the horizontal axis in each of these figures is the ratio of the incident wave intensity I_{in} to a reference intensity I_0. The vertical axis is an integer Flag which is either 1 or 0 corresponding to convergence or non-convergence, as defined by the stop criterion

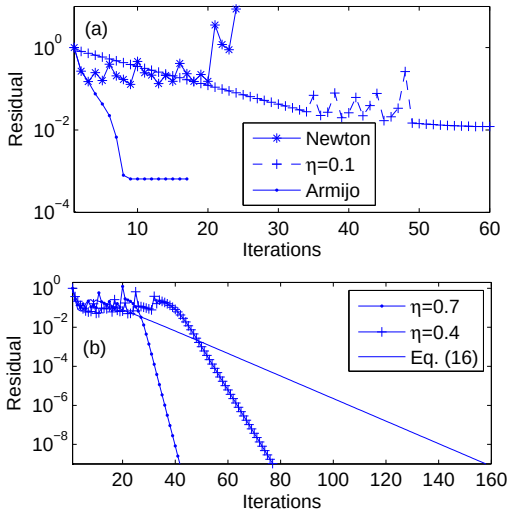

Figure 6: Normalized residuals of the iterations. (a) non-convergent cases: Newton's method, damped Newton's method with Armijo rule and with $\eta = 0.1$; (b) convergent cases: damped Newton's method with $\eta = 0.4$ and 0.7, and our method Eq. (16).

(28) and the maximum of 2000 iterations. All these iterative methods work well for a relatively small incident wave intensity satisfying $I_{in} \leq 10.6 I_0$, and the iterations converge to the solution corresponding to the lower branch in Fig. 3. Newton's method is the most efficient for these cases. On the other hand, if $I_{in} > 10.6 I_0$, the solution goes to the upper branch in Fig. 3. In that case, Newton's method and damped Newton's method with a constant η have rather unpredictable convergence behavior. The damped Newton's method with Armijo rule always fails, since it attempts to minimize the residual in each step and converges to a nonzero local minimum of the residual. As shown in Fig. 5(f), our iterative method always converges. The results in Fig. 5 are only for $8 \leq I_{in}/I_0 \leq 15$, but we have tested our method up to $I_{in} = 150 I_0$, and it always converges starting with the zero initial guess and the number of iterations is always less than 200.

To take a closer look at the convergence processes, we consider the particular case of $I_{in} = 11.4 I_0$. For this incident wave, Newton's method, damped Newton's method with Armijo rule, and damped Newton's method with constant $\eta = 0.1$ do not converge. The normalized residuals $||\boldsymbol{f}(\boldsymbol{u}^{(l)}||/||A\boldsymbol{g}||$ of these three methods are shown in Fig. 6(a). It can be seen that the normalized residual of Newton's method changes erratically with the iterations and

exceeds 10 at the 25th iteration. The damped Newton's method with Armijo rule reduces the residual quickly for the first a few iterations, but then settles down to a constant. The damped Newton's method for constant η fails to converge for $\eta = 0.1$, but converges for $\eta = 0.4$ and $\eta = 0.7$. In Fig. 6, we show the convergence processes for the two latter cases and for our method given in Eq. (16). These methods show linear convergence rates. To satisfy the stop criterion (28), i.e., to reach a relative error of 10^{-9}, our method requires 158 iterations, while the damped Newton's method for $\eta = 0.4$ and 0.7 requires 78 and 48 iterations, respectively. However, the required CPU time for one iteration of our method is less than one half of that for Newton's method or damped Newton's method. This is related to the difference for solving a complex linear system and a real linear system of twice the size. As a result, in terms of the total CPU time, our method actually outperforms the damped Newton's method for $\eta = 0.4$.

To analyze the dependence of the solutions on the amplitude of the incident wave, and to obtain the curve shown in Fig. 3, it is natural to use a numerical continuation scheme where the obtained solution for one incident wave is used as the initial guess to solve the NLH for a slightly different incident wave. Starting from a small I_{in} and increase I_{in} by $0.1I_0$ in each step, all iterative methods are able to determine the lower branch of Fig. 3. However, when I_{in} is increased from $10.6I_0$ to $10.7I_0$, the solution jumps to the upper branch, then Newton's method, the damped Newton's method with Armijo rule, and the damped Newton's method for $\eta = 0.1$, 0.4 and 0.7 all fail to converge. Our method converges, i.e., reaches the stop criterion, in 184 iterations. Actually, the damped Newton's method for $\eta = 0.05$ also converges, but it only converges in 1443 iterations, and is about 18 times slower than our method.

Since our method converges for $I_{in} \geq 10.7I_0$, we can use the continuation scheme to calculation the upper branch of the solution curve by decreasing or increasing I_{in} slightly in each step. The middle branch is more difficult to calculate. We choose $I_{in} = 7I_0$, and try to find the solution corresponding to point B in Fig. 3. There is no straightforward way to choose the initial guess so that the iterations converge to point B. Our initial guess is the solution corresponding to point C multiplied by a real constant. For a properly chosen constant, our iterative method converges to the solution correspond to point B. After that, we can easily find the middle branch by decreasing or increasing I_{in} slightly in each step.

7. Conclusion

In this paper, we developed a new iterative method, Eq. (16), for solving the 2D NLH. The method is specially designed for the NLH and it has excellent global convergence behavior. As shown by numerical results involving a nonlinear circular cylinder, when good initial guesses near the exact solution are not available, Newton's method and damped Newton's method often fail to converge, but it appears that our method always converges. To take advantage of the local quadratic convergence of Newton's method, our method can be used in the first stage of a hybrid method to find a sufficiently good approximation, and Newton's method can be used in the second stage to further improve the solution. Further studies are needed to gain a better understanding of the new iterative method. Numerical results show a linear convergence rate, but a theoretical justification is yet to be developed. The most interesting property of our method is its robust convergence behavior. However, the reasons for its robustness are still unknown.

So far, we have only considered a relatively small problem where the linear system in each iteration can be easily solved. For problems where the size of the nonlinear domain is much larger than the wavelength, the linear system becomes the main bottleneck, and quasi-Newton and inexact Newton methods become important. We expect that our method still has the advantage in global convergence for large problems, and believe that it is worthwhile to develop variants of our method, similar to quasi-Newton and inexact Newton methods, that are more efficient for large scale problems. Our study is further limited by the 2D NLH itself. For 2D problems in the strongly nonlinear regime, a system of equations is needed when the harmonic generation process becomes important. For 3D nonlinear optical problems, the scalar model is usually not valid, and it is necessary to solve the full system of nonlinear Maxwell's equations. Clearly, it is important to develop methods similar to Eq. (16), with a good global convergence property, for 2D systems and 3D Maxwell's equations.

References

[1] R. W. Boyd, Nonlinear Optics, 3rd ed. Academic, 2008.

[2] B. Maes, P. Bienstman, and R. Baets, Modeling of Kerr nonlinear photonic components with mode expansion, Opt. Quant. Electron. **36**, 15–24 (2004).

[3] G. Bao, Y. Lia, and H. Wu, Numerical solution of nonlinear diffraction problems, J. Comput. Appl. Math. **190**, 170–189 (2006).

[4] H. Gibbs, Optical Bistability: Controlling Light with Light, Academic, 1985.

[5] E. Centeno and D. Felbacq, Optical bistability in finite-size nonlinear bidimensional photonic crystals doped by a microcavity, Phys. Rev. B **62**, R7683–R7686 (2000).

[6] J. Bravo-Abad, A. Rodriguez, P. Bermel, S. G. Johnson, J. D. Joannopoulos, and M. Soljačić, Enhance nonlinear optics in photonic-crystal microcavities, Opt. Express **15**, 16161–16176 (2007).

[7] Z. Xu and G. Bao, A numerical scheme for nonlinear Helmholtz equations with strong nonlinear optical effects, J. Opt. Soc. Am. A **27**, 2347–2353 (2010).

[8] L. Yuan and Y. Y. Lu, Efficient numerical method for analyzing optical bistability in photonic crystal microcavities, Opt. Express **21**, 11952–11964 (2013).

[9] G. I. Stegeman and M. Segev, Optical spatial solitons and their interactions: universality and diversity, Science **286**, 1518 (1999).

[10] G. Fibich and S. Tsynkov, Numerical simulation of nonlinear Helmholtz equation using nonorthogonal expansions, J. Comput. Phys. **210**, 183–224 (2005).

[11] G. Baruch, G. Fibich, and S. Tsynkov, High-order numerical method for nonlinear Helmholtz equation with material discontinuities in one space dimension, J. Comput. Phys. **227**, 820–850 (2007).

[12] G. Baruch, G. Fibich, and S. Tsynkov, Simulations of the nonlinear Helmholtz equation: arrest of beam collapse, nonparaxial solitons and counter-propagating beams, Opt. Express **16**, 13323–13329 (2008).

[13] G. Baruch, G. Fibich, and S. Tsynkov, A high-order numerical method for the nonlinear Helmholtz equation in multidimensional layered media, J. Comput. Phys. **228**, 3789–3815 (2009).

[14] J.P. Torres, J. Boyce, and R.Y. Chiao, Bilateral symmetry breaking in a nonlinear Fabry-Perot cavity exhibiting optical tristability, Phys. Rev. Lett. **83**, 4293–4296 (1999).

[15] B. Maes, P. Bienstman, and R. Baets, Symmetry breaking with coupled Fano resonances, Opt. Express **16**, 3069–3076 (2008).

[16] E. Bulgakov, K. Pichugin, and A. Sadreev, Symmetry breaking for transmission in a photonic waveguide coupled with two off-channel nonlinear defects, Phys. Rev. B **83**, 045109 (2011).

[17] E. N. Bulgakov and A. F. Sadreev, Switching through symmetry breaking for transmission in a T-shaped photonic waveguide coupled with two identical nonlinear micro-cavities, Phys. Rev. B **84**, 155304 (2011).

[18] L. Yuan and Y. Y. Lu, Bilateral symmetry breaking in nonlinear circular cylinders, Opt. Express **22**, 30128–30136 (2014).

[19] M. Soljačić and J. D. Joannopoulos, Enhancement of nonlinear effects using photonic crystals, Nat. Mater. **3**, 211–219 (2004).

[20] M. F. Yanik, S. Fan, and M. Soljačić, High-contrast all-optical bistable switching in photonic crystal microcavities, Appl. Phys. Lett. **83**, 2739–2741 (2003).

[21] H. C. Chang and L. C. Chen, Simple numerical approach for determining the optical response of a nonlinear dielectric slab for both TE and TM waves, Phys. Rev. B **43**, 9436–9441 (1991).

[22] H. V. Baghdasaryan and T. M. Knyazyan, Problem of plane EM wave self-action in multilayer structure: an exact solution, Opt. Quantum Electron. **31**, 1059 (1999).

[23] M. Midrio, Shooting technique for the computation of plane-wave reflection and transmission through one-dimensional nonlinear inhomogeneous dielectric structures, J. Opt. Soc. Am. B **18**, 1866 (2001).

[24] P. K. Kwan and Y. Y. Lu, Computing optical bistability in one-dimensional nonlinear structures, Optics Communications **238**, 169–175 (2004).

[25] C. T. Kelley, Iterative methods for linear and nonlinear equations, Society for Industrial and Applied Mathematics, Philadelphia, 1995.

[26] L. N. Trefethen, Spectral Methods in MATLAB, Society for Industrial and Applied Mathematics, 2000.